In search of a universal rough wall model

Xiang I. A. Yang
Mechanical Engineering,
Pennsylvania State University
University Park, PA, 16802, USA
Email: xzy48@psu.edu

Wen Zhang
Guangdong Provincial Key Laboratory
of Turbulence Research and Applications,
Southern University of Science and Technology
Shenzhen, 518055, PR China

Junlin Yuan
Mechanical Engineering,
Michigan State University
East Lansing, MI, 48824, USA

Robert F. Kunz
Mechanical Engineering,
Pennsylvania State University
University Park, PA, 16802, USA

ABSTRACT

This work compares various existing rough-wall models on a large collection of rough surfaces with different characteristics and studies the potentials of these models in accommodating new datasets. We consider three empirical roughness correlations, two physics-based models, and one data-driven machine-learning model on 68 rough surfaces inside and outside the Roughness Database [roughnessdatabase.org]. Results show that correlation-type models and machine-learning models do not extrapolate outside the dataset against which they are calibrated or trained. In contrast, the physics-based sheltering model performs well in extrapolation. Re-calibrating a roughness correlation against a large dataset proves unfruitful. However, re-training a machine learning model yields good results. We do not pursue further re-training and re-calibrating of a physics-based model, as it requires new physical insights. Overall, our findings suggest that a universal rough-wall model is yet to be found. The capability of extrapolation will likely come from incorporating physics. Data, on the other hand, benefits machine learning models.

NOMENCLATURE

A Log law intercept

A_f Frontal area

A_p Planar area

A_t Total planar area

B Log law intercept

C_d Drag coefficient

ES Effective slope

ES_x Streamwise effective slope

ES_z Spanwise effective slope

h Surface elevation

k Roughness height

k_c Maximum peak-to-trough height

k_{rms} Root-mean-square height

k_s Equivalent sand-grain roughness height

$k_{s,p}$ Predicted equivalent sand-grain roughness height

k_t Average peak-to-trough height obtained from a surface tile of size $\delta \times \delta$

Ra Mean roughness height

Sk Skewness

Ku Kurtosis

U Mean streamwise velocity

y Wall-normal distance

y_0 Equivalent roughness height

ΔU^+ Roughness function

κ von Kármán constant

λ_f Solidity

λ_p Planar density

1 INTRODUCTION

1.1 Background

Roughness is common: barnacles on ship surfaces [1, 2] and canopies in the atmospheric boundary layer [3] are examples of surface roughness. They inflict a drag penalty on the fluid flow; predicting that drag penalty is one objective of rough-wall modeling. Rough-wall modeling has received sustained attention in the past few decades [4, 5, 6, 7, 8]. Most existing rough-wall models assume fully rough turbulent flows. The premise of rough-wall modeling is the logarithmic law [9, 10, 11]

$$U^+ = \kappa^{-1} \ln(y^+ - d^+) + B - \Delta U^+ \tag{1}$$

where U is the mean flow velocity, the superscript $+$ denotes normalization by wall units, y is the wall-normal coordinate, d is the zero-plane displacement height (often neglected,) $\kappa \approx 0.4$ is the von Kármán constant, $B \approx 5$ is the log-law intercept in the smooth-wall flow counterpart, and ΔU^+ is the roughness function [12, 13]. $\Delta U^+ = 0$ for a flat-plate boundary layer, and is a logarithmic function of k_s^+ in the fully-rough regime. Equation 1 can be re-written as

$$U^+ = \kappa^{-1} \ln\left[(y - d)/k_s\right] + A, \tag{2}$$

or

$$U^+ = \kappa^{-1} \ln\left[(y - d)/y_0\right]. \tag{3}$$

Here, k_s is the equivalent sand-grain roughness height; it is related to ΔU^+ as

$$\Delta U^+ = \kappa^{-1} \ln({k_s}^+) + B - A, \tag{4}$$

Reference	Model type	Roughness statistics	Number of parameters	Interpretable	Responsive to arrangement
MacDonald 1998	Physics-based	0.05<λp=λf<0.9	3	Yes	Partly
Yang et al 2016	Physics-based	0.03<λp<0.4	2	Yes	Yes
Forooghi et al 2017	Correlation	-0.35<Sk<0.68 0.2<ES<0.89	5	No	No
Barros et al 2018	Correlation	-0.03<Sk<0.11 0.09<ES<0.14	2	No	No
Flack et al 2020	Correlation	-0.7<Sk<1.51 0.16<ES<0.74	7	No	No
Jouybari et al 2021	Data-driven	-1.45<Sk<2.37 0.068<ES<1.1	521	No	No

Table 1. Details of the rough wall models. The sheltering model by Yang et al. 2016 [14] contains two parameters: the wake expansion rate and the sectional drag coefficient of an isolated, un-sheltered roughness element. The physics-based model in MacDonald 1998 [15] is partly responsive to changes in roughness arrangements because one can assign different drag coefficients to different roughness arrangements. The data-driven model is a feed-forward neural network. The many hidden layers and the weights and biases give rise to a large number of parameters.

and $A = 8.5$ is a constant; y_0 is the equivalent roughness height, and it is related to k_s as

$$y_0 = k_s \exp(-\kappa A) \approx k_s/30. \tag{5}$$

Hence, in the fully-rough regime, knowing ΔU^+ is equivalent to knowing k_s, and knowing k_s is equivalent to knowing y_0. The objective of rough-wall modeling is to predict ΔU^+, or equivalently, y_0 or k_s, based on roughness morphology. However, predicting ΔU^+ is non-trivial because of the infinite range of possible roughness geometries. The purpose of this work is to collect as much rough-wall data as we can, and test selected existing rough-wall models on these rough walls.

1.2 Rough-wall models

The existing rough-wall models can be put into three categories: correlation-type models, physics-based models, and data-driven models. In the following, we review the three modeling approaches.

Correlation-type rough-wall models map roughness statistics to the equivalent sandgrain roughness height according to

$$k_s = f\left(\text{roughness statistics}\right). \tag{6}$$

The function form f is usually heuristic and contains a number of adjustable constants. These constants are calibrated against a given dataset. Early correlations like the ones in Refs. [16, 17, 18] contain one input, e.g., the solidity, where $k_s = f(\lambda_f)$. More recent correlations contain more inputs [19], e.g., k_{rms}, k_{sk}, and ES. A lot of thought has been put into the roughness statistics required within the function f. Chung et al. argued that a good correlation must contain some measure of the height, solidity and planar coverage of the roughness [6]. Flack & Chung reviewed the existing empirical correlations in [7]. Testing all these empirical correlations is a formidable task and does not necessarily return commensurate insight. In this work, we will test the correlations in Refs. [20, 19, 21]. These three correlations read:

$$k_s/k_z = 1.07\left(0.67Sk^2 + 0.93Sk + 1.3\right)\left(1 - e^{-3.5ES}\right), \tag{7}$$

which is from Ref. [19],

$$k_s/k_{rms} = 3.41(1 + Sk)^{0.61}, \tag{8}$$

which is from Ref. [21], and

$$k_s/k_{rms} = \begin{cases} 2.48(1 + Sk)^{2.24} & Sk > 0, \\ 2.11, & Sk = 0, \\ 2.73(1 + Sk)^{-0.45} & Sk < 0. \end{cases} \tag{9}$$

which is from Ref. [20]. These correlations represent the current thinking [6] and have shown good predictive power. We will test the off-the-shelf versions of these correlations and adjust the parameters to test their potentials to fit new data.

Physics-based models are motivated by physical considerations such as conservation laws, flow sheltering, and velocity scalings [22, 23, 24]. Prior knowledge is often needed for the drag coefficient as a function of roughness solidity and geometry, etc. Here, we will test the two physics-based models in Refs. [14, 15]. The model in Ref. [15] assumes the logarithmic law and a constant stress layer. Knowledge of the roughness' drag coefficient as a function of the roughness' solidity is required. Such knowledge is usually not available for an arbitrary rough surface, which

Roughness	References	Measurement type
Bi-directional sanded	Schultz & Flack 2007	Experiment
Cuboids	Yang et al 2016	Simulation
Grit-blasted	Thakkar 2017	Simulation
Fractal-like cubes	Yang & Meneveau 2017	Simulation
Power-law	Barros et al 2018	Experiment
Gaussian	Flack et al 2020	Experiment
Multi-scale cuboids	Medjnoun et al 2021	Experiment
Truncated cones	Womack et al 2022	Experiment
Deep (slender) rectangular	Zhang et al 2022	Simulation

Table 2. Rough wall details.

limits the applications of the model. The sheltering model in Ref. [14] invokes momentum and mass conservation, the exponential law in the roughness layer [25, 26], and the log law in the outer layer. The model explicitly accounts for the sheltering among roughness elements [27]. Knowledge of the drag coefficient of an un-sheltered roughness element is required—unlike the sectional drag coefficient, the drag coefficient of an isolated roughness element is usually available [28]. The two physics-based models have been tested for cuboidal roughness. We will test if they predict k_s of other types of roughness. The reader is directed to Refs. [14, 15] for further details of the two models.

Data-driven models share the philosophy of correlation-type models. However, rather than specifying the function, data-driven models delegate that task to, e.g., an artificial neural network (ANN). We will test two versions of a data-driven rough-wall model: the deep neural network developed in Ref. [29], which was trained on 45 rough walls, and that re-trained on a larger dataset presented herein.

Table 1 shows further details of the roughness models, including the type of the model, the reference, the value ranges of the roughness statistics considered when these models were developed, the number of model parameters, whether the model is interpretable, whether the model is computationally efficient, and whether the model responds to changes in roughness arrangement. For a machine learning model that employs a neural network, the number of parameters is the number of weights and biases in the network, which is usually large.

1.3 Rough walls

We limit ourselves to homogeneous roughness whose in-plane scales are smaller than the boundary-layer height. Large in-plane scales do not usually contribute significantly to drag and can be removed by filtering [35, 36]. 68 rough walls are considered. Most of these rough walls and their respective flow data can be found in the online Roughness Database [roughnessdatabase.org]. We assume full knowledge of the roughness geometry and measure roughness statistics across the entire surface rather than on a few cuts through the surface [30, 21, 20]. Table

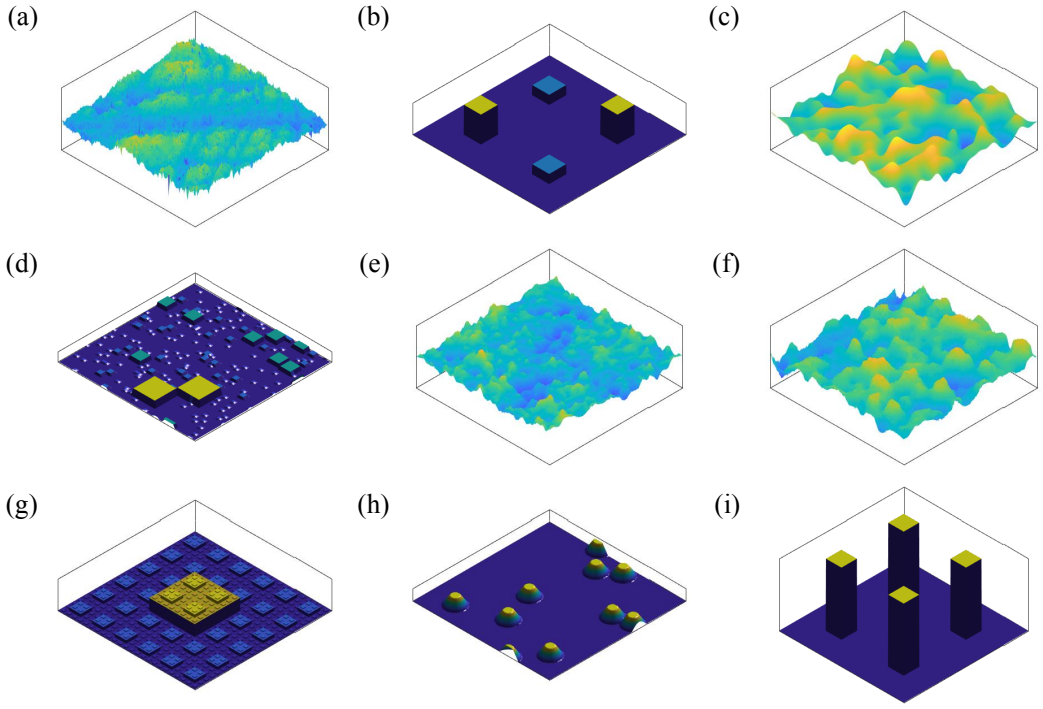

Fig. 1. Rough wall topology: (a) Bi-directional sanded roughness in Ref. [30], (b) cuboidal roughness in Ref. [14], (c) grit-blasted roughness in Ref. [31], (d) fractal-like roughness in Ref. [32], (e) power-law roughness in Ref. [21], (f) Gaussian roughness in Ref. [20], (g) LEGO like roughness in Ref. [33], (h) truncated cones in Ref. [34], (i) deep rectangular roughness in Ref. [26].

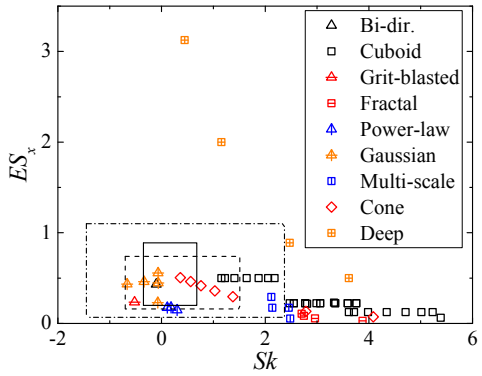

Fig. 2. Effective slope and skewness of the rough walls in Table 2. The solid, dashed, and dash-dotted squares indicate the parameter ranges used to develop the correlations in Ref. [19], Ref. [20], and Ref. [29], respectively.

2 tabulates the roughness type, the reference, and whether the flow is experimentally measured or computed in a simulation. The bi-directional-sanded surface in Ref. [30], the grit-blasted roughness in Ref. [31], the fractal-like multi-scale roughness in Ref. [32], the power-law roughness in Ref. [21], and the Gaussian roughness in Ref. [20] are irregular roughness geometries. The cuboidal roughness in Ref. [14], LEGO-like roughness in Ref. [33], truncated cones in Ref. [34], and deep rectangular roughness in Ref. [26] are regular roughness geometries. Figure 1 shows the

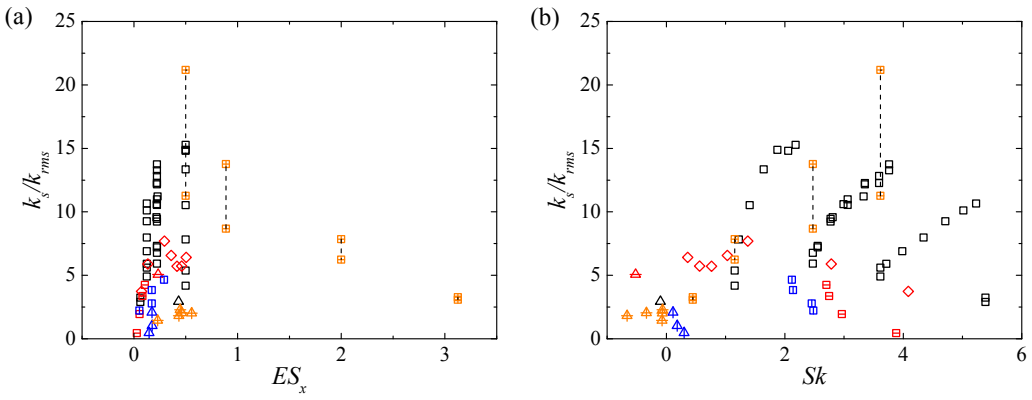

Fig. 3. k_s/k_{rms} as a function of (a) ES_x or (b) S_k for all the rough surfaces. The symbols are the same as in Fig 2. The dashed lines connects two surfaces that are differ only in their arrangements (one is aligned, and one is staggered).

topology of a few rough surfaces.

Figure 2 shows the ranges of the effective slope, ES_x, and the roughness skewness, Sk, of these rough surfaces. Most rough walls are within the range $0 \leq ES_x \leq 0.5$ except for the deep rectangular roughness in Ref. [26], whose ES_x is as large as 3. Most surfaces are positively skewed with $0 \leq Sk \leq 6$, except for the grit-blasted roughness in Ref. [31], and some of the Gaussian roughness in Ref. [20], which are negatively skewed. Figure 3 shows the normalized equivalent sandgrain roughness height k_s/k_{rms} as a function of the effective slope ES and the roughness skewness Sk, where k_{rms} is the root mean square of the surface roughness. We see that the data covers a wide range of k_s/k_{rms} values, and, as Chuang et al. pointed out, k_s/k_{rme} is not solely determined by either ES or Sk [6].

1.4 This work

We will test the 7 models in Table 1, as they are, on the 68 rough walls in Table 2. As the datasets used to develop these models were more limited than the present test data, the models will be extrapolating. Consequently, errors larger than those reported in these studies may be expected. Next, we will re-calibrate the correlation-type models and re-train the data-driven model and test how well re-calibrated and re-trained models fit the data. The exercise will assess the potential of the two types of models in accommodating new datasets. The two physics-based models are not altered/re-calibrated. Altering a physics-based model requires new physical insights, which are not always available.

The work will provide insights into the advantages and disadvantages of the various modeling approaches. The hope is that such knowledge will point us toward a universal rough-wall model.

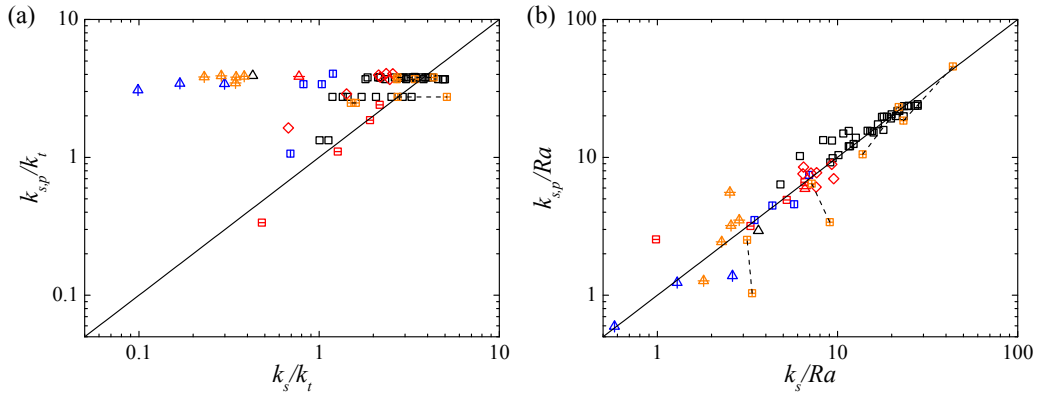

Fig. 4. Predicted k_s as a function of the measured k_s for (a) the model in Ref. [15], and (b) the model in Ref. [14]. The symbols are the same as in Fig 2. Here, $k_{s,p}$ is the predicted equivalent sandgrain roughness height, and K_s is the data.

2 RESULTS

We apply off-the-shelf roughness models in section 1.2 to the rough wall morphologies in section 1.3. The results are presented in section 2.1. The correlation in Ref. [21] and the neural network in Ref. [29] are re-calibrated and re-trained against the rough walls of section 1.3. The results of the re-calibrated and re-trained models are shown in section 2.2. The results are presented on a log scale since it is $\log(k_s^+)$ rather than k_s^+ that appears in the mean flow scaling.

2.1 Rough-wall models as they are

The predictions of the physics-based models are compared to data in Fig. 4. The model in Ref. [15] is responsive to only the roughness solidity λ_f and is agnostic to changes in roughness skewness, roughness height, or roughness arrangement. Consequently, the model predicts similar $k_{s,p}$ for a wide range of roughness whose k_s varies by almost two orders of magnitude. The sheltering model in Ref. [14] extrapolates well and returns reasonably good estimates for all types of roughness. In particular, the model responds to changes in roughness arrangements, yielding less flow sheltering and therefore larger k_s for staggered roughness and more flow sheltering and therefore smaller k_s for aligned roughness. While this captures the correct physics when the roughness elements are closely packed [37], the physics is such that secondary flow arises when the roughness elements are sparsely packed [38]. These secondary flows bring high momentum fluid to within the roughness layer, leading to similar k_s for staggered and aligned roughness, which is not captured by the sheltering model. Errors are also found for multi-scale roughness, for which the physics is unclear and therefore not accounted for in the model. Figure 5 shows the results for the three correlation-type models. The correlation-type models do not perform well. The k_s estimates are one to two orders of magnitude off for many of the surfaces. Lastly, Fig. 6 shows the results for the machine learning model. The model performs reasonably

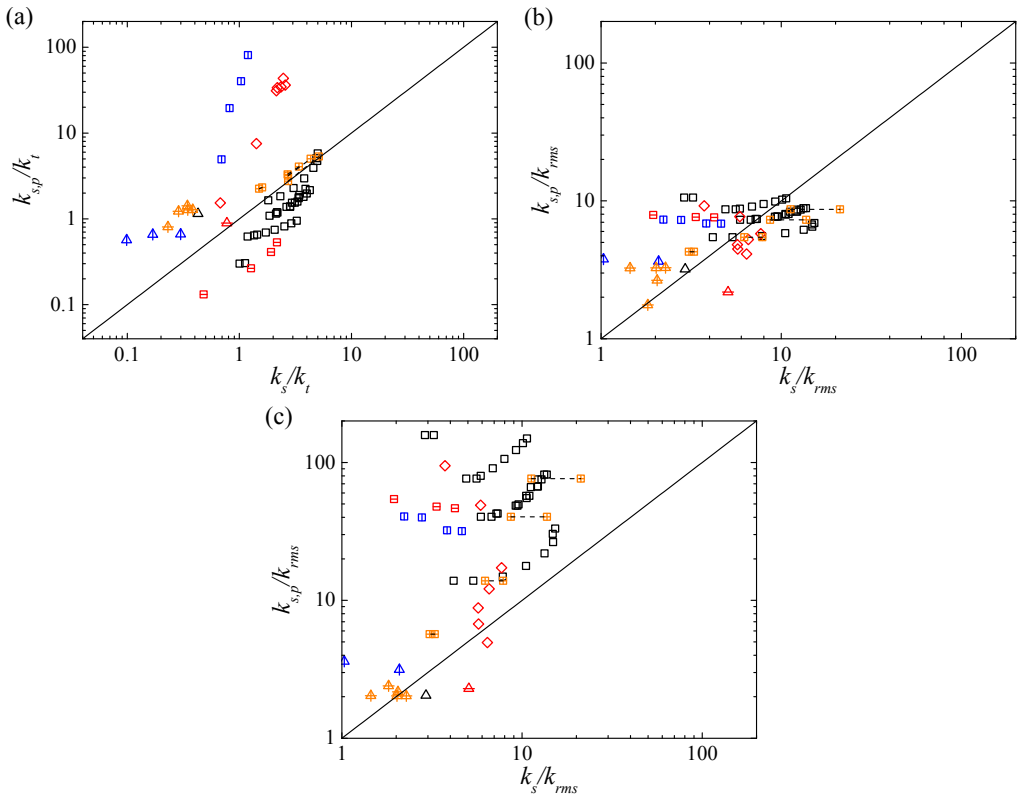

Fig. 5. Same as Fig. 4 but for (a) the model in Ref. [19], (b) the model in Ref. [21], (c) the model in Ref. [20].

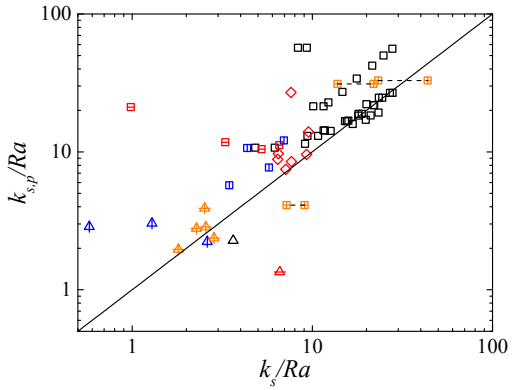

Fig. 6. Same as Fig. 4 but for the model in Ref. [29].

well. Extrapolation is still a challenge, like any other data-driven models, and there are significant errors in surfaces with multi-scale roughness and cubical roughness. It is difficult to interpret the correlation models and the machine learning model, and a more detailed discussion of these results are not pursued here.

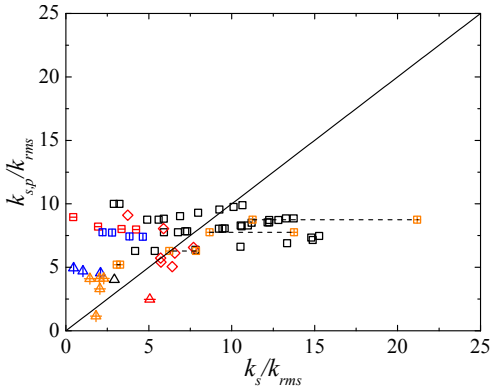

Fig. 7. Same as Fig. 5 (b) but for the re-calibrated correlation $k_{s,p}/k_{rms} = 4.96(0.68 + Sk)^{0.39}$.

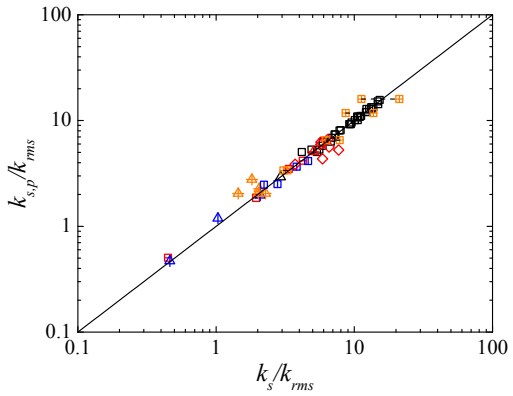

Fig. 8. Same as Fig. 4 but for the re-calibrated correlation $k_{s,p}/k_{rms} = C_1(C_2 + Sk)^{C_3}$. The values of the three constants are tabulated in Table 3.

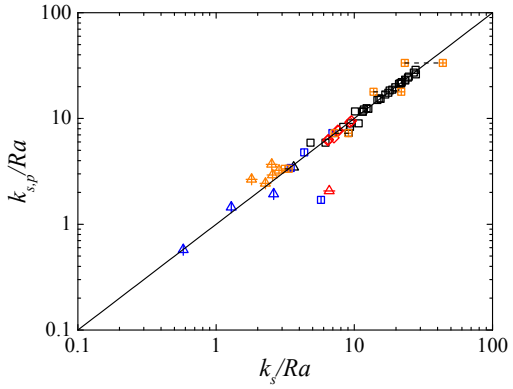

Fig. 9. Same as Fig. 4 but for the re-trained neural network.

2.2 Re-calibration and re-training

The correlations in Refs. [21, 20, 19] and the neural network in Ref. [29] are re-calibrated and re-trained against the rough walls in section 1.3. First, we re-calibrate the correlation in Ref. [21] against all 68 surfaces by adjusting

Roughness	Reference	C1	C2	C3
Bi-directional sanded	Schultz & Flack 2007	3.6	0.68	0.39
Cuboids, $\lambda_p = 0.06$	Yang et al. 2016	6.9	-3.0	0.54
Cuboids, $\lambda_p = 0.11$		12	-2.4	0.31
Cuboids, $\lambda_p = 0.25$		15	-1.1	0.27
Gaussian cubes		2.2	1.0	1.1
Grit-blasted, S8	Thakkar 2017	10	0.68	0.39
Fractal-like cuboids	Yang & Meneveau 2017	0.89	-2.4	-1.4
Power-law	Barros et al 2018	4.0	1.0	6.0
Gaussian	Flack et al 2020	2.0	1.0	-0.30
Multi-scale cuboids	Medjnoun et al 2021	2.1	-2.1	-0.17
Truncated cones	Womack et al 2022	7.5	1.0	-0.41
Deep rectangular	Zhang et al 2022	5.2	0.15	0.85

Table 3. Roughness and the re-calibrated constants. We re-calibrate against cubes of different surface coverage densities in Ref. [14] separately. "Gaussian cube" is cubes whose heights satisfy the Gaussian distribution.

C_1, C_2, and C_3 in $k_{s,p}/k_{rms} = C_1(C_2 + Sk)^{C_3}$ such that the re-calibrated correlation best fits the data. The results are shown in Fig. 7. Comparing Figs. 7 to 5(b), we see no significant improvement. This is not unexpected. The correlation contains k_{rms}, Sk, and 3 constants and therefore has very limited descriptive power. Next, we re-calibrate the correlation for each type of roughness separately. Table 3 tabulates the model constants and the roughness used for re-calibration. The results are shown in Fig. 8. The model constants vary drastically from one dataset to another. Nonetheless, this time, we see a close agreement between the predicted k_s and the data. Repeating the above exercise for the two correlations in Refs. [19, 20] gives very similar results (not shown here for brevity.) Last, we retrain the neural network in Ref. [29] against all 68 rough surfaces. The results are shown in Fig. 9, and we see a close agreement between the network's predictions and the data without separately re-training for each type of roughness. However, this particular neural network does not capture the difference among cuboidal roughness with varying element arrangements, as it does not use surface inputs that describe such differences.

3 CONCLUSIONS

This work tests 7 rough wall models on 68 rough surfaces inside and outside the Roughness Database. The study covers physics-based roughness models, correlation-type models, and data-driven models. Regular and irregular roughness are considered, as well as single-scale and multi-scale roughness. The off-the-shelf sheltering model in Ref. [14] works very well. Although it was originally developed for cuboidal roughness, the model gives accurate k_s estimates for most rough walls tested, responding accurately to changes in essentially all single-point roughness statistics and roughness' arrangements. However, a physics-based model is as effective as the scope of physics it incorporates; for the present models, sparse and fractal roughness may pose particular challenges. The off-the-shelf

empirical correlations in Refs. [19, 21, 20] work poorly, yielding k_s estimates that are often one to two orders of magnitudes off for some correlations. The off-the-shelf machine learning model in Ref. [29] also yields significant errors for some types of roughness due to extrapolation (like any other machine learning models).

The many rough surfaces and comprehensive surface data in the Roughness Database allow for easy re-calibration. We re-calibrate and re-train the empirical correlation in [21] and the neural network in [29]. Retraining the correlation against all 68 rough walls yields no significant improvement. However, when the correlation is re-calibrated separately for Gaussian roughness, power-law roughness, and fractal roughness, etc., it gives accurate k_s predictions. On the other hand, re-training the machine learning model against all 68 rough walls proves to be fruitful—although the re-trained model does not respond to changes in roughness arrangement due to the lack of such surface features in model inputs.

We summarize our observations below. Correlation-type models are easy to implement. They give accurate predictions if calibrated against and applied to the same type of roughness. Physics-based models generalize better than correlation-type models and machine-learning models, but more data does not necessarily help improve the performance of physics-based models and, instead, missing physics need to be identified and incorporated. On the other hand, more data directly translates to improved model performance for machine learning models. This provides an interesting possibility for rough-wall modeling: a good rough-wall model might be the results of a lot of data and limited flow physics.

ACKNOWLEDGEMENTS

Yang acknowledges NSF grant no. 2231037 and ONR grant no. N000142012315 for financial support. Kunz acknowledges ?? Zhang acknowledges NSFC grant no. 12102168.

REFERENCES

[1] Schultz, M., Bendick, J., Holm, E., and Hertel, W., 2011, "Economic impact of biofouling on a naval surface ship," *Biofouling,* **27**(1), p. 8798.

[2] Monty, J., Dogan, E., Hanson, R., Scardino, A., Ganapathisubramani, B., and Hutchins, N., 2016, "An assessment of the ship drag penalty arising from light calcareous tubeworm fouling," *Biofouling,* **32**(4), pp. 451–464.

[3] Barlow, J., and Coceal, O., 2008, A review of urban roughness sublayer turbulence.

[4] Jimenez, J., 2004, "Turbulent flows over rough walls," *Annu. Rev. Fluid Mech.,* **36**, p. 17396.

[5] Flack, K. A., and Schultz, M. P., 2010, "Review of hydraulic roughness scales in the fully rough regime," *J. Fluids Eng.,* **132**, p. 041203.

[6] Chung, D., Hutchins, N., Schultz, M. P., and Flack, K. A., 2021, "Predicting the drag of rough surfaces," *Annual Review of Fluid Mechanics,* **53**, p. 439471.

[7] Flack, K. A., and Chung, D., 2022, "Important parameters for a predictive model of ks for zero pressure gradient flows," In AIAA SciTech, AIAA.

[8] Klewicki, J. C., 2010, "Reynolds number dependence, scaling, and dynamics of turbulent boundary layers," *J. Fluids Eng.,* **132**(9).

[9] Townsend, A. A., 1976, *The Structure of Turbulent Shear Flow,2nd edn.* Cambridge University Press.

[10] Raupach, M., Antonia, R., and Rajagopalan, S., 1991, "Rough-wall turbulent boundary layers," *Appl. Mech. Rev.,* **44**, p. 125.

[11] Marusic, I., Monty, J. P., Hultmark, M., and Smits, A. J., 2013, "On the logarithmic region in wall turbulence," *J. Fluid Mech.,* **716**.

[12] Clauser, F. H., 1954, "Turbulent boundary layers in adverse pressure gradients," *J. Aeronaut. Sci.,* **21**, p. 91108.

[13] Hama, F. R., 1954, "Boundary-layer characteristics for smooth and rough surfaces," *Trans. SNAME,* **62**, p. 333351.

[14] Yang, X. I. A., Sadique, J., Mittal, R., and Meneveau, C., 2016, "Exponential roughness layer and analytical model for turbulent boundary layer flow over rectangular-prism roughness elements," *J. Fluid Mech.,* **789**, p. 127165.

[15] Macdonald, R. W., Griffiths, R. F., and Hall, D. J., 1998, "An improved method for the estimation of surface roughness of obstacle arrays," *Atmospheric environment,* **32**, pp. 1857–1864.

[16] Simpson, R. L., 1973, "A generalized correlation of roughness density effects on the turbulent boundary layer.," *AIAA J.,* **11**(2), pp. 242–244.

[17] Sigal, A., and Danberg, J. E., 1990, "New correlation of roughness density effect on the turbulent boundary layer," *AIAA J.,* **28**(3), pp. 554–556.

[18] D.R. Waigh, R. K., 1998, "Improved aerodynamic characterization of regular three-dimensional roughness," *AIAA J.,* **36**, pp. 1117–1119.

[19] Forooghi, P., Stroh, A., Magagnato, F., Jakirlic, S., and Frohnapfel, B., 2017, "Toward a universal roughness correlation," *J. Fluids Eng.,* **139**, p. 121201.

[20] Flack, K. A., Schultz, M. P., and Barros, J. M., 2020, "Skin friction measurements of systematically-varied roughness: probing the role of roughness amplitude and skewness," *Flow Turbul. Combust.,* **104**, p. 317329.

[21] Barros, J. M., Schultz, M. P., and Flack, K. A., 2018, "Measurements of skin-friction of systematically generated surface roughness," *Int J Heat Fluid Flow,* **72**, pp. 1–7.

[22] Harman, I., and Finnigan, J., 2007, "A simple unified theory for flow in the canopy and roughness sublayer," *Boundary-Layer Meteorol.,* **123**, pp. 339–363.

[23] Aupoix, B., 2016, "Revisiting the discrete element method for predictions of flows over rough surfaces," *J. Fluids Eng.,* **138**(3).

[24] Altland, S., Xu, H. H., Yang, X. I., and Kunz, R., 2022, "Modeling of cube array roughness: Rans, large eddy simulation, and direct numerical simulation," *J. Fluids Eng.,* **144**(6), p. 061106.

[25] Cionco, R., 1965, "A mathematical model for air flow in a vegetative canopy," *J. Appl. Meteorol.,* **4**, pp. 517–522.

[26] Zhang, W., Zhu, X., Yang, X. I. A., and Wan, M., 2022, "Evidence for raupach et al.s mixing-layer analogy in deep homogeneous urban-canopy flows," *J. Fluid Mech.,* **944**(A46).

[27] Raupach, M., 1992, "Drag and drag partition on rough surfaces," *Boundary-Layer Meteorol.,* **60**, p. 375395.

[28] Schlichting, H., 1979, *Boundary-Layer Theory* McGraw-Hill, New York.

[29] Jouybari, M. A., Yuan, J., Brereton, G. J., and Murillo, M. S., 2021, "Data-driven prediction of the equivalent sand-grain height in rough-wall turbulent flows," *J. Fluid Mech.,* **912**(A8).

[30] Schultz, M. P., and Flack, K. A., 2007, "The rough-wall turbulent boundary layer from the hydraulically smooth to the fully rough regime," *J. Fluid Mech.,* **580**, p. 381405.

[31] Thakkar, M., Busse, A., and Sandham, N., 2017, "Surface correlations of hydrodynamic drag for transitionally rough engineering surfaces," *J. Turbul,* **18**, pp. 138–169.

[32] Yang, X. I. A., and Meneveau, C., 2017, "Modelling turbulent boundary layer flow over fractal-like multiscale terrain using large-eddy simulations and analytical tools," *Philosophical Transactions of the Royal Society A: Mathematical, Physical and Engineering Sciences,* **375**, p. 20160098.

[33] Medjnoun, T., Rodriguez-Lopez, E., Ferreira, M. A., Griffiths, T., Meyers, J., and Ganapathisubramani, B., 2021, "Turbulent boundary-layer flow over regular multiscale roughness," *J. Fluid Mech.,* **917**, p. A1.

[34] Womack, K. M., Volino, R. J., Meneveau, C., and Schultz, M. P., 2022, "Turbulent boundary layer flow over regularly and irregularly arranged truncated cone surfaces," *J. Fluid Mech.,* **933**(A38).

[35] Yuan, J., and Piomelli, U., 2014, "Estimation and prediction of the roughness function on realistic surfaces," *J. Turbul,* **15**, p. 350365.

[36] Barros, J. M., Schultz, M. P., and Flack, K. A., 2018, "Measurements of skin-friction of systematically generated surface roughness," *Int J Heat Fluid Flow,* **72**, pp. 1–7.

[37] Xu, H. H., Altland, S. J., Yang, X. I., and Kunz, R. F., 2021, "Flow over closely packed cubical roughness," *J. Fluid Mech.,* **920**.

[38] Yang, X., Xu, H., Huang, X., and Ge, M.-W., 2019, "Drag forces on sparsely packed cube arrays," *J. Fluid*

Mech., **880**, pp. 992–1019.